Journal of Applied Sciences

ISSN 1812-5654

science alert

ANSInet
an open access publisher
http://ansinet.com

Journal of Applied Sciences 12 (10): 902-910, 2012
ISSN 1812-5654 / DOI: 10.3923/jas.2012.902.910

Computational Modeling of High Temperature Processing Maps for Microalloyed Al-Cu-Mg Alloys Using Artificial Neural Networks

Sanjib Banerjee, Nastagis Niyaz Ahmed, Pranjal Bhuyan and Subhashish Baruah
Department of Mechanical Engineering, Tezpur University, Tezpur, 784028, India

Abstract: High temperature deformation behavior of Al-5.9, Cu-0.5%, Mg alloy and Al-5.9, Cu-0.5%, Mg alloy containing 0.06 wt.% Sn was studied by hot compression tests conducted at different temperatures and strain rates. Trace content of Sn resulted in a significant increase of flow stress for various processing conditions. Artificial Neural Network (ANN) modeling was applied providing excellent prediction of flow stress at different combinations of strain, strain rate and deformation temperature. While validation, it was possible to predict 100 and 89% of the flow stress values of the respective alloys within an error less than±10%. The flow stress data thus generated using the ANN architectures was used to develop power dissipation efficiency maps, instability maps and subsequently the processing maps which would delineate the process domains for safe metal working. Optimum hot processing window was suggested for the investigated alloys, providing intelligent processing and manufacturing system of these wrought microalloyed Al alloys, extensively used in aircraft and space applications. The power dissipation efficiency maps revealed a maximum efficiency of 60% for the alloy without Sn content, while a comparatively lower value of 40% for the microalloyed material. The instability maps generated for the alloy containing Sn, revealed only one instability regime. The safe regimes for hot working of the base alloy without Sn content were observed at (i) very low strain rate (<0.003 sec^{-1}) with temperature <450°C and (ii) high temperature (>400°C) with strain rate >0.02 sec^{-1}. The safe processing zone of the alloy with trace content of Sn, is at low strain rate (<0.01 sec^{-1}) for the entire range of temperatures studied. Microstructural analysis confirmed that dynamic recovery (DRV) and dynamic recrystallization (DRX) characterized the safe processing regimes of both the alloys. Instability during hot deformation was observed to be driven mainly by shear band formation and/or intercrystalline cracking for the investigated Al alloys.

Key words: Aluminum alloy, microalloying, high temperature deformation behavior, artificial neural network, processing map

INTRODUCTION

The high demand and interest in aircraft and space related applications in the recent years have resulted in a thrust for development of light weight alloys exhibiting high specific strength, reasonable ductility, high fracture toughness and good corrosion resistance properties (Heinz *et al*., 2000; ASM International Handbook Committee, 1990). Aluminum alloys, especially the wrought and precipitation strengthened Al-Cu (2xxx), Al-Mg-Si (6xxx) and Al-Zn-Mg-Cu (7xxx) series of alloys, were developed because of their high strength to weight ratio. The 2xxx series of Al alloys are used for high strength structural applications such as aircraft fittings and wheels, rocket fins, military vehicles and bridges, forgings for trucks, etc., the Al-Cu-Mg alloys of 2124, 2219 and 2618 are extensively used even in aerospace structures demanding good heat resistance properties up to 150°C (Sukumaran *et al*., 2008; Raju *et al*., 2007).

The mechanical properties of these alloys are affected even by minute variations in composition, strain history and the microstructure resulting from the thermo-mechanical treatment imparted before the final use. Subsequently, the present research trend is to develop increased strength combined with properties of reasonable toughness and low density by the addition of trace elements (microalloying i.e., alloying elements <0.1 wt. %) like Sn, In, Cd, Ag, Si, etc., in to the alloy matrix (Hirosawa *et al*., 2000; Sercombe and Schaffer, 1999).

These wrought alloys need to undergo a thermo-mechanical treatment prior to their final use, to reduce the defects (viz. segregations, dendrite structures, gas defects, inclusions etc.) induced during casting. This deformation process is generally carried out at high homologous temperatures i.e., $T/T_m > 0.5$ where, T and T_m are the absolute working temperature and melting temperature of the material, respectively. A clear understanding of the process variables and material

Corresponding Author: Sanjib Banerjee, Department of Mechanical Engineering, Tezpur University, Tezpur, 784028, India

parameters is required for successfully deforming these materials within a range of strain rates ($\dot{\epsilon}$) and processing temperatures (T).

'Workability' is an important parameter in mechanical working which refers to the relative ease with which a metal can be shaped through plastic deformation without introducing any defect. One of the most important methods to demonstrate hot workability of a material is by means of processing maps. Various models were developed through decades, for understanding the deformation behavior of metallic alloys, viz. Kinetic models proposed by Flynn *et al.* (1961) and reviewed by Jonas *et al.* (1969), Ashby maps (Atomistic mechanism maps) Frost and Ashby (1982) representing the materials response in the form of deformation mechanism maps and finally (Raj, 1981) to construct processing maps. Dynamic Materials Model (DMM) was developed (Prasad and Sasidhara, 1997; Prasad *et al.*, 1984) for studying the workability parameter, based on principles of continuum mechanics of large plastic flow using the concepts of physical systems modeling and extremum principles of irreversible thermodynamics. This model for hot deformation is expected to predict: (1) The response of the workpiece material in terms of microstructural evolution, (2) Optimum process parameters without trial and error and (3) Process limits for controlling the manufacturing environment. The approaches available for modeling hot deformation behavior have been reviewed earlier by Prasad (1990) and Kutumarao and Rajagopalachary (1996). It was possible by DMM to bridge the principles of continuum mechanics of large plastic deformation and microstructural evolution in materials.

The major irreversible changes in the microstructure and their salient features are: (i) Dynamic recrystallization (DRX) in the temperature range of 0.7-0.8 T_m and at intermediate $\dot{\epsilon}$ and low $\dot{\epsilon}$ for low and high Stacking Fault Energy (SFE) materials, respectively (Prasad and Ravichandran, 1991) (ii) Dynamic recovery (DRV) in the homologous temperature range of 0.4-0.6, (iii) Adiabatic shear bands at higher $\dot{\epsilon}$ (Prasad *et al.*, 2000), (iv) Void formation at high $\dot{\epsilon}$ and low T (Raj, 1981; Prasad and Sasidhara, 1997), (v) Intercrystalline cracking at higher T and $\dot{\epsilon}$ and (vi) Wedge cracking and superplasticity in the temperature range of 0.7-0.8 T_m and at $\dot{\epsilon}$<0.01 sec^{-1} (Prasad and Sasidhara, 1997).

True stress (σ) vs. true strain (ε) curves provide microstructural information related to the mechanisms of hot deformation. Different 'safe' and 'damage' mechanisms occur at various zones of $\dot{\epsilon}$ and deformation T, although sometimes a combination of these mechanisms can even occur. The safe mechanisms comprise of DRX and DRV (Ravichandran and Prasad, 1991). The superplastic deformation is also considered to be safe while the others are to be avoided during hot deformation. However, for optimizing hot workability and controlling the microstructure, DRX is a chosen domain. A processing map is an explicit representation of the response of a material in terms of microstructural mechanisms, to the imposed process parameters. It is obtained by the superimposition of a power dissipation map and instability map developed on the basis of DMM (Prasad and Sasidhara, 1997). The variation of efficiency of power dissipation with T and $\dot{\epsilon}$ constitutes a power dissipation map which exhibits various domains in which specific microstructural mechanisms occur. The efficiency map itself represents the power transactions within a continuum and the understanding of its origin and its interpretation in terms of atomistic mechanisms requires a correlation with some of the concepts of irreversible thermodynamics. It helps in interpreting the microstructures resulting from hot deformation as 'dissipative and characterizes them in terms of atomistic mechanisms. Instability map separates out the regions of stable and unstable flow. Industrial metal working processes require the information provided by the processing maps. For newer materials, the process can be designed to suit the constitutive requirements of the material from the viewpoint of optimum workability and microstructural control. In addition, these maps can be used to optimize existing processes which can help improve the product quality and yield. Defects arising during hot deformation processing can be avoided with the knowledge of the limiting T and $\dot{\epsilon}$ conditions which lead to the flow instabilities.

Processing maps for a large number of metals, alloys, intermetallics and metal matrix composites have been systematically compiled along with a summary of metallurgical interpretations (Prasad and Sasidhara, 1997). However, only a few reports are available on the effect of alloying elements and the corresponding microstructural changes and processing maps of some commercial Al alloys (Cavaliere, 2002; Kaibyshev *et al.*, 2002). The purpose of the present study was therefore, to investigate the influence of trace additions of tin (Sn) on the high temperature deformation/flow behavior and workability of Al-Cu-Mg alloys and subsequently to generate the processing maps for these alloys. Selecting elemental Sn becomes a worthy of investigation since Sn has already been reported to affect the mechanical properties of some Al alloys (Sercombe and Schaffer, 1999). The deformation behavior of the alloys was studied by hot compression tests performed at various temperatures and strain rates. Neural network has been successfully demonstrated as a

Neural network has been successfully demonstrated as a more robust technique than any other conventional methods for generating the processing maps (Robi and Dixit, 2003). The flow stresses (σ) was hence modeled by Artificial Neural Network (ANN) and the generated σ values were used to develop high temperature processing maps for the alloys. To the best of the investigator's knowledge, this is the first attempt made to propose the optimum hot processing window for industrial production of these highly applicable wrought 2xxx series Al-Cu-Mg alloys microalloyed with Sn and thereby to provide an intelligent processing and manufacturing system for the same.

EXPERIMENTAL PROCEDURES AND METHODOLOGY ADOPTED

Al: 5.9 wt.%, Cu: 0.5 wt.%, Mg alloy (Alloy-A, composition close to 2219 Al alloy) and Al: 5.9 wt.%, Cu: 0.5 wt.%, Mg alloy containing 0.06 wt.% Sn (Alloy-B) were prepared from aluminum ingots by a casting route. The cylindrical samples cast in graphite moulds were machined to 12 mm diameter and 200 mm length. The machined sample rods were then homogenized at 510°C for 10 h to reduce the non-homogeneity in composition and microstructure resulting from coring and segregation during solidification. Cylindrical specimens having dimensions of 10 mm diameter and 15 mm height were then machined from the annealed rods for hot compression testing.

High temperature compression tests were carried out using a servo-hydraulic controlled dynamic 100 kN capacity universal testing machine (UTM, make: INSTRON, Model: 8801). A split-type resistance heated furnace was fabricated and attached to the UTM to maintain a constant test temperature. The cross head velocity of the UTM actuator was varied such that a constant true strain rate was maintained during the entire duration of each compression test. The actuator displacement at any instant of time was controlled by the closed loop servo-hydraulic control of the UTM using MAX™ software. The strain rates ($\dot{\epsilon}$) and temperatures (T), at which the tests were performed, are given in Table 1. The tests were carried out up to a true strain (ϵ) of 0.6. The load vs. displacement plots for all the tests were obtained during the compression tests, from which the true stress (σ) vs. true strain (ε) curves were obtained. The flow stresses for each combination of strain, strain rate and temperature were determined from these plots.

The flow stress of the two alloys was then modeled by artificial neural network (ANN). The ANN modeling was carried out by the Multiple Layer Perception (MLP) feed forward back propagation network. The input layer consisting of three neurons (ε, $\dot{\epsilon}$ and T) and the flow stress, σ, in the output layer formed the data sets for training the network. The 'Neural Network' tool box available with the MATLAB (Release 7) software package was used for the present modeling. Training of the neural network was done using the ANN tool kit of MATLAB software, using trainlm function. Trainlm is a network training function that updates weights and bias values in a back propagation algorithm according to Levenberg-Marquardt optimization. Single layer hidden neurons were used in the network architecture. The number of neurons in the hidden layer, the transfer functions at the input-to-hidden layer and hidden-to-output layer were optimized by trial and error method during the network training and testing stages. The Mean Square Error (MSE) during the training and testing was determined for each trial. The network architecture was finally frozen based on the minimum MSE value obtained during both the training and testing stages. Out of the total 120 number of data sets of each alloy, 48 and 36 data sets were used for, respectively training and testing. Eighteen data sets from the remaining were used for evaluation using the trained network architecture. Once the proper network architecture was arrived at for an alloy, the flow stress (σ) could be successfully predicted for any combination of input parameters (viz. ε, $\dot{\epsilon}$ and T), within the specified domain range.

Table 1: Strain rates and temperatures of the hot compression tests

$\dot{\epsilon}$ (sec^{-1})	T (°C)
0.001, 0.01, 0.1 and 1.0	300, 350, 400, 450 and 500

The flow stress values as predicted by ANN were used to generate the processing maps for the investigated alloys. These maps can be generated from hot compression tests data acquired at constant $\dot{\epsilon}$ under isothermal conditions. The relevant calculations were performed using MATLAB™ software toolkit. The basis for obtaining the power dissipation map is Dynamic Materials Model (DMM) and their interpretations which have been discussed in detail by (Prasad and Sasidhara, 1997; Prasad *et al*., 1984). The efficiency of power dissipation for a nonlinear dissipator may be expressed as a dimensionless parameter η which is the relative rate of entropy production during hot deformation characterizing the dissipative microstructure under different T and $\dot{\epsilon}$ conditions.

The efficiency of power dissipation according to the DMM model and as proposed by Prasad *et al*. (1984) is:

$$\eta = \frac{2m}{m+1} \quad (1)$$

The term m, the strain rate sensitivity factor, is strain rate dependent. As proposed by Murty *et al.* (2000), the efficiency of power dissipation can be obtained from the flow stress as:

$$\eta = 2\left(1 - \frac{1}{\sigma \dot{\varepsilon}}\int_0^{\dot{\varepsilon}} \sigma \, d\dot{\varepsilon}\right) \quad (2)$$

As proposed by Prasad *et al.* (1984), the following metallurgical instability criterion was subsequently arrived:

$$\xi\left(\dot{\varepsilon}\right) = \frac{\partial \ln\left(\frac{m}{m+1}\right)}{\partial \ln \dot{\varepsilon}} + m \leq 0 \quad (3)$$

The parameter $\xi(\dot{\epsilon})$ is evaluated as a function of T and $\dot{\epsilon}$ to obtain an instability map, indicating metallurgical instability during plastic flow occurring at regimes where its values are negative. In a power dissipation map, the efficiency of power dissipation is contour plotted as a function of T and $\dot{\epsilon}$ at a particular true strain value. Instability map separates out the regions of stable and unstable flow. Processing map is then obtained by the superimposition of a power dissipation map and instability map developed on the basis of DMM (Prasad and Sasidhara, 1997).

Immediately after the test, each cylindrical compressed sample was water quenched in situ to avoid any metadynamic process, sectioned parallel to the axis and prepared for Optical Microscope (OM) using standard metallographic technique. The polished specimens were then observed under an upright optical microscope (Carl Ziess, Axiotech) equipped with Kontron KS-400 image analysis system, in order to identify the irreversible changes induced in the microstructure as a result of deforming them to a true stain value of 0.6.

RESULTS AND DISCUSSION

Flow stress behavior: The flow curves (σ vs. ϵ) obtained for Alloy-A at various strain rates ($\dot{\epsilon}$) and deformation temperatures (T) are shown in Fig. 1. During the plastic deformation, both the materials strain-hardened with increase in strain. At the onset of plastic deformation, σ increased rapidly. The σ increased at a decreasing rate with increase in ε, till a maximum stress, or peak flow stress (σ_p) was reached. Beyond the peak strain (ϵ_p), i.e., the strain to reach the maximum stress, the σ either decreased with increase in ε or nearly saturated. The former case was when the softening rate was higher than the work hardening rate while the latter phenomenon

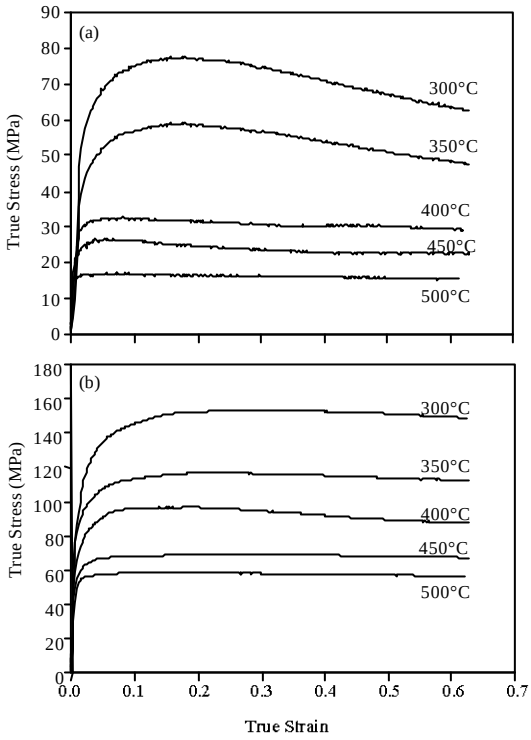

Fig. 1(a-b): Flow curves at strain rates of (a) 0.001 sec^{-1} and (b) 1.0 sec^{-1}

occurred when the softening rate was equal to the work hardening rate (Cavaliere, 2002; Kaibyshev *et al.*, 2002; Robi and Dixit, 2003; Murty *et al.*, 2000; Medina and Hernandez, 1996). However, the flow softening after attaining the peak stress was considerable only at the lowest $\dot{\epsilon}$ (0.001 sec^{-1}) studied for both the alloys. From Fig. 1, it is also evident that the σ value increased with increase in $\dot{\epsilon}$, while decrease in deformation T which is a general trend in high temperature deformation (Zhang *et al.*, 2007; Liu *et al.*, 2009). For almost all the combinations of ε, $\dot{\epsilon}$ and T, the flow stress of the investigated Al-Cu-Mg alloy system was observed to increase significantly due to the addition of 0.06 wt.% Sn. From the point of design applicability, the Al-Cu-Mg alloy microalloyed with Sn, possesses higher strength attributed to the second phase precipitation but is relatively difficult to deform as revealed from the higher values of flow stress and activation energy for hot deformation (Banerjee *et al.*, 2010; Banerjee *et al.*, 2012).

Generation of processing maps for hot workability: The ANN modeling carried out provided excellent prediction of flow stress, σ (ε, $\dot{\epsilon}$, T) in the process domain of

investigation. During validation, it was observed that 18 and 16 out of 18 data points fall within ±10% deviation error line respectively for Alloy-A and Alloy-B. The root mean square (RMS) errors were registered as 2.37 and 5.40 for these two alloys while validation. The σ values thus predicted using the frozen ANN architectures, were used to generate processing maps which would delineate the process domains for safe metal working and thus would be of considerable importance for industrial processing of these wrought alloys.

The efficiency of power dissipation (η) and strain rate sensitivity factor (m) of the two alloys were contour plotted as a function of $\dot{\epsilon}$ and deformation T, for true strain (ε) values of 0.2, 0.4 and 0.6. Figure 2 show the contour plots for η and m at various T and $\dot{\epsilon}$ values for Alloy-A after deforming it to a ϵ of 0.2. The following observations are evident from these Fig. 2a-d: (i) At T<~370°C and for $\dot{\epsilon}$>0.1 sec^{-1}, η<20%. In this regime, the values of m are very low. (ii) At T above 450°C, η>20% for the entire range of $\dot{\epsilon}$. The m <0.3 in this region. (iii) For $\dot{\epsilon}$ in the range of 0.001-0.01 sec^{-1} and T<420°C, η>30%. The m>0.1 in this regime. (iv) η>45% at T<425°C and $\dot{\epsilon}$<0.003 sec^{-1}. The η contours in this domain are generally widely spaced. In this regime, m>0.2. (v) For $\dot{\epsilon}$ <0.03 sec^{-1} and T between 400 and 480°C, values of η and m show an increasing trend with decreasing $\dot{\epsilon}$. This could probably correspond to the wedge cracking regime. DRX generally occurs at regimes where maximum efficiency of power dissipation is between 50-55% for high stacking fault energy (SFE) materials like Al. From the above observations, it is also evident that the efficiency of power dissipation is higher for the regime having higher m values. Figure 2 (b, c) show the isoefficiency plots obtained for Alloy-A when deformed to ϵ of 0.4 and 0.6, respectively. As is evident from the figures, the values of power dissipation efficiency increased with increase in ϵ from 0.2 to 0.6.

Isoefficiency plots obtained for Alloy-B after deformation to ϵ values of 0.2 and 0.6 are shown in Fig. 3. The η contours are more widely spaced for Alloys B, as compared to those of the base alloy (Alloy-A). In the $\dot{\epsilon}$ range 0.158 to 0.025 sec^{-1}, the power dissipation efficiency contours are more closely spaced compared to the other regions of the plot. The efficiency of power dissipation continuously increases with increase in T and/or decrease in $\dot{\epsilon}$. Maximum efficiency of power dissipation was obtained as 35 and 40% for ϵ values of 0.2 and 0.6, respectively. Such high value is observed at T>480°C and for 0.0032 sec^{-1} <$\dot{\epsilon}$ <0.01 sec^{-1}. Inspection of the plots obtained at different ϵ values indicates similar features, though the values of the power dissipation efficiency increased with increase in ϵ. The maximum in the efficiency of power dissipation is obtained where m has its maximum value. The process parameters at which the efficiency of power dissipation is maximum for the two investigated alloys are listed in Table 2 along with the corresponding m values.

A convenient way of locating the optimum processing conditions is to locate regimes where the isoefficiency contours are widely spaced. Several dynamic

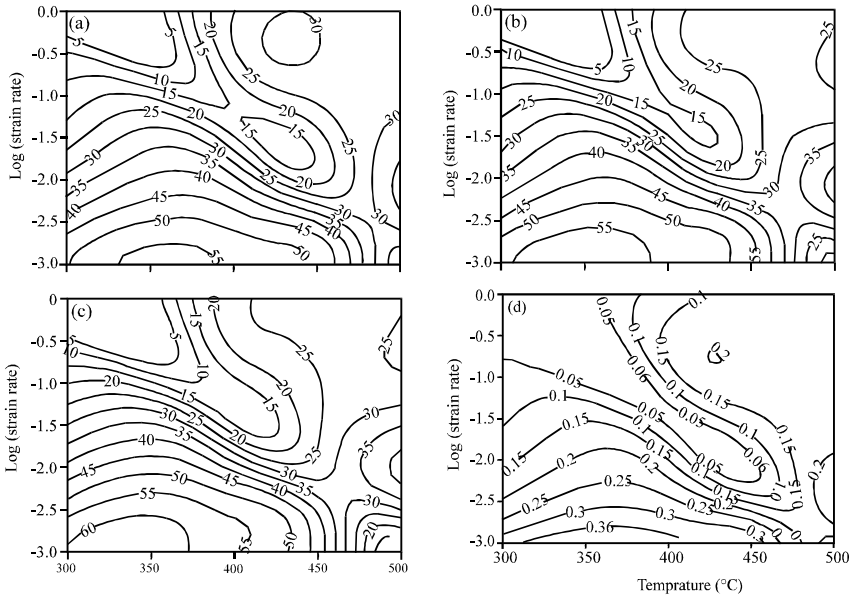

Fig. 2(a-d): Contour plots of η at ϵ of (a) 0.2 (b) 0.4 (c) 0.6 and (d) contour plot of m at ϵ of 0.2 for Alloy-A

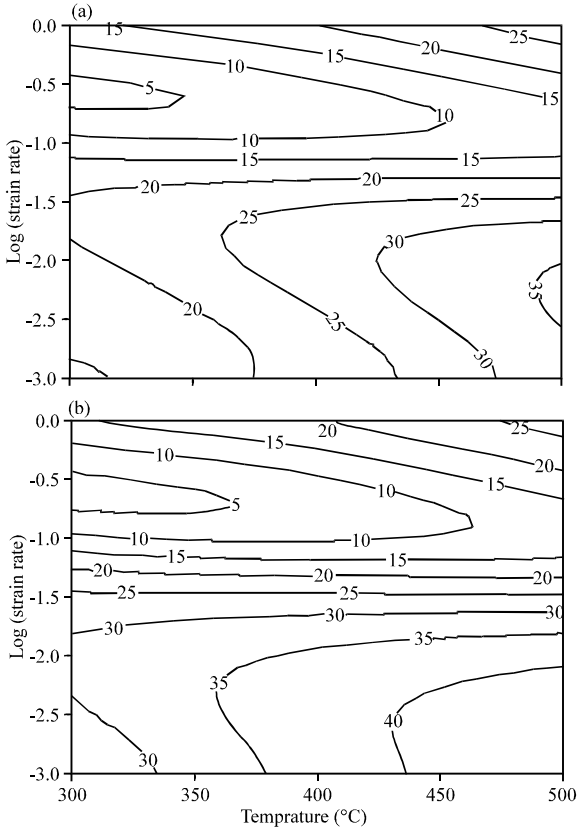

Fig. 3(a-b): Contour plots of η for Alloy-B at ϵ of (a) 0.2 and (b) 0.6

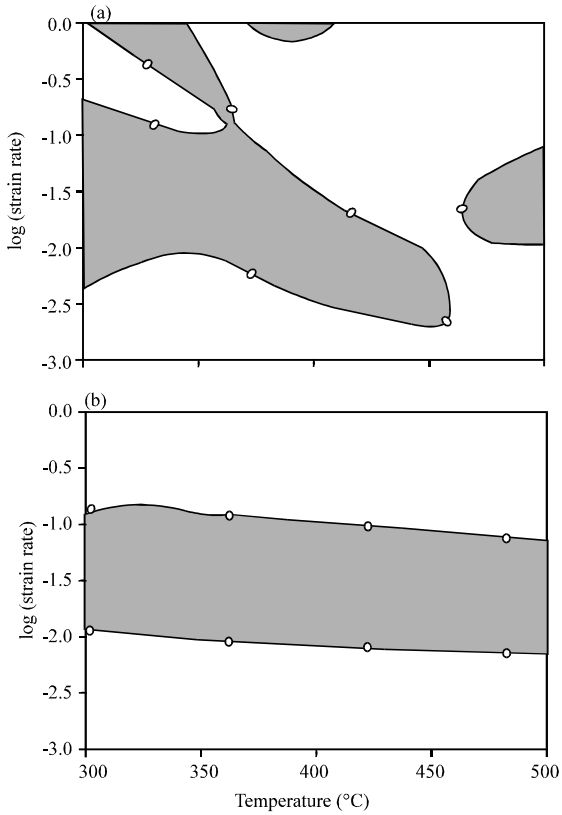

Fig. 4(a-b): Instability (shaded) regions for (a) Alloy-A and (b) Alloy-B at ϵ of 0.6

Table 2: Process parameters for maximum power dissipation efficiency values of the investigated alloys

Sample ID	Maximum power dissipation efficiency (%)	Strain-rate ranges (sec^{-1})	Temperature ranges (°C)	Maximum strain rate sensitivity factor (m)
Alloy-A	60	0.001-0.003	300-400	0.45
Alloy-B	40	0.001-0.01	440-500	0.25

metallurgical processes contribute to power dissipation during the hot deformation of materials. These metallurgical processes have characteristic ranges of efficiencies of power dissipation. Depending upon the microstructure, some of these processes may occur simultaneously and/or interactively. When more than one major power dissipation processes having different characteristics occur simultaneously, the energy of dissipation of one of the processes may become equal to that of another. The regime indicating metallurgical instability during plastic flow can be obtained by the instability condition as given by the Eq. (3).

Figure 4 shows instability maps for Alloy-A and Alloy-B at ϵ of 0.6. The regions in the $\dot{\epsilon}$-T plane where the values of parameter ζ are negative (shaded regions in the figures) are indicative of unstable metal flow. The boundary lines separating the stable and unstable flow regions indicate ζ = 0, as shown in the instability maps. The flow instabilities arise due to irreversible changes in the microstructure during plastic flow of the material. The figures indicate the regions where the contour lines of efficiency of power dissipation are closely spaced as the regimes of plastic instability. The two regions where Alloy-A can be considered as safe for hot working are: (i) region existing at high T (> ~420°C) for $\dot{\epsilon} > 0.03\ sec^{-1}$ and (ii) low $\dot{\epsilon}$ region (<0.0019 sec^{-1}) existing at all temperatures studied. Though the nature of these two stable regions remains almost similar, stability is obtained in the case of the latter even for a slight increase in $\dot{\epsilon}$. It can also be noted from Fig. 4, that the Alloy-A has four regions of instability at a ϵ value of 0.6. With increase in ϵ, the instability region at the highest temperature (500°C at a ϵ = 0.2) increases in size and spreads to lower temperatures (say, up to 460°C at a ϵ = 0.6). The instability maps generated for Alloy-B with 0.06 wt.% Sn, showed only one instability regime which is a different feature as compared to that of Alloy-A. With Sn addition, the

instability regions are found to lie almost parallel to the isoefficiency lines.

Figure 5 shows the processing maps for Alloy-A and Alloy-B at a ϵ value of 0.6, obtained by superimposing the corresponding power dissipation maps and instability maps of these two alloys. The shaded areas in figures hence indicate the unstable regions. The Fig. 5(a) indicates lower values of efficiency of power dissipation for unstable regions as compared to the adjacent stable regions in case of Alloy-A. The stable regions of Alloy-A after a ϵ of 0.6 are observed at: (i) High T (>400°C) and for $0.02 < \dot{\epsilon} < 1$ sec^{-1} and (ii) Very low $\dot{\epsilon}$ (<0.003 sec^{-1}) at all temperatures studied. From the processing map, it can be concluded that Alloy-A can be safely deformed under the above mentioned conditions. Figure 5(b) reveals the stable regions of Alloy-B which are observed for: (i) $\dot{\epsilon}$>0.1 sec^{-1} and (ii) $\dot{\epsilon}$<0.01 s^{-1} for the entire range of temperatures studied in both the cases.

Microstructural evolution: Power dissipation map can provide insight on various dissipative microstructures during the hot working process. To study the dissipative microstructures formed during hot deformation, the microstructures of specimens deformed to a ϵ of 0.6 under various $\dot{\epsilon}$ and processing *T* were observed using optical microscope. For Alloy-A, features of flow localization/shear band formation were observed in the sample deformed at 300°C and $\dot{\epsilon}$ of 0.1 sec^{-1}. Since, this process condition falls in the major instability regime [the large shaded region in Fig. 5(a), this shaded region can be considered as an instability arising due to shear band formation. The microstructure of the sample deformed at T = 300°C and $\dot{\epsilon}$ of 0.001 sec^{-1}, reveals formation of subgrains, possibly resulting from dynamic recovery (DRV). It may be mentioned that the processing temperature of T = 300°C falls well within the homologous temperature range of 0.4-0.6 of the investigated Al-Cu-Mg alloy system. The microstructure of the alloy deformed at 500°C at a $\dot{\epsilon}$ of 0.001 sec^{-1} reveals occurrence of dynamic recrystallization (DRX). Though the processing map for Alloy-A Fig. 5a indicates the regime of high T and very low $\dot{\epsilon}$ as safe, the isoefficiency contour plots indicate steep gradient in the efficiency values. This is further substantiated by the fact that though the microstructure of the alloy deformed at 500°C at a $\dot{\epsilon}$ of 0.001 sec^{-1} reveals DRX, wedge cracks can also be observed along the grain boundaries. This clearly shows initiation of defects in this regime under the above process conditions. Hence, deformation of Alloy-A at $0.001 < \dot{\epsilon} < 0.003$ and T range of 450-500°C is to be avoided.

Figure 5(b) shows only one regime of flow instability for Alloy-B. The flow instability regime corresponds to

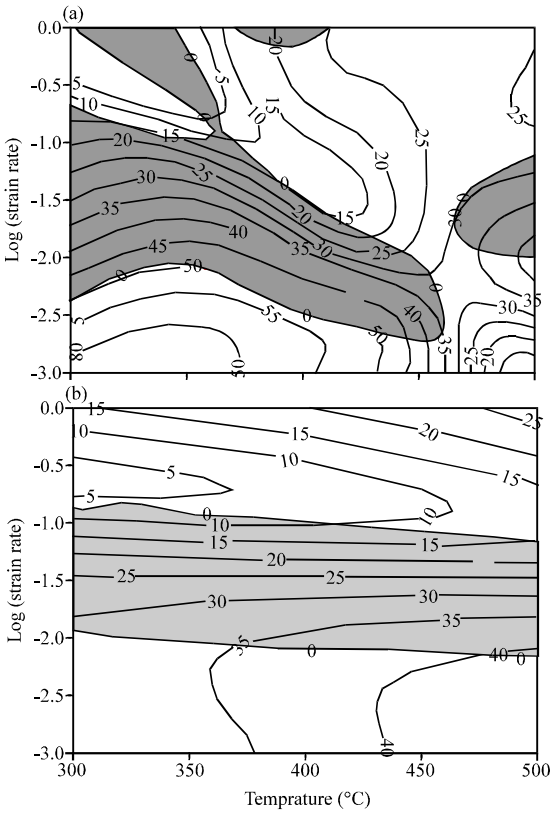

Fig. 5(a-b): Processing maps for (a) Alloy-A (b) Alloy-B at ϵ of 0.6

$\dot{\epsilon}$ in the range of 0.1 to 0.01 sec^{-1} and T in the range of 300-500°C. Microscopic studies of the samples deformed at 350°C and $\dot{\epsilon}$ of 0.1 sec^{-1} as well as at 500°C and $\dot{\epsilon}$ of 0.01 sec^{-1}, reveal adiabatic shear band formation as the major metallurgical phenomenon causing flow instability in this regime. Similar to Alloy-A, the metallurgical phenomenon occurring at $\dot{\epsilon}$<0.01 sec^{-1} have been subsequently identified as DRV and DRX at processing temperatures of 300 and 500°C, respectively. Although the region at 500°C and higher $\dot{\epsilon}$ of 1.0 sec^{-1}, is marked as a stable region in the instability map of Fig. 4, microscopic investigation revealed features of intercrystalline cracking which is generally encountered at higher T and higher $\dot{\epsilon}$ values. Presence of Sn favours the formation of the low melting point phase, at the grain boundaries which was substantiated in separate investigations (Banerjee *et al*., 2010; Banerjee *et al*., 2012).

The above studies indicate that the safe regimes for hot working of Alloy-A are: (i) Very low $\dot{\epsilon}$(<0.003 sec^{-1}) at T <450°C and (ii) High T (>400°C) and $0.02 < \dot{\epsilon} < 1$ sec^{-1}. On the other hand, the safe processing regime for Alloy-B may be proposed at low $\dot{\epsilon}$ (<0.01 sec^{-1}) and for the entire range of temperatures studied. Unlike Alloy-A, DRX in

Alloy-B could comfortably continue, devoid of any simultaneous instability phenomenon, at higher deforming temperatures. It may therefore be observed that most stable regions of the investigated alloys are characterized by DRV or DRX. As a consequence of these phenomenon, as shown in Figure 1, considerable flow softening was observed in both the alloys deforming at lowest strain rate of 0.001 sec^{-1}. The safe processing zone primarily lies at lower regimes of strain rate which is extended up to higher deformation temperatures, with the trace addition of Sn. There have been few reports in some earlier literatures where DRX in Al alloys has been shown to occur at lower $\dot{\varepsilon}$ and is sensitive to the impurity content (Prasad and Sasidhara, 1997). In another study of Al with different purities in the temperature range of 250-600°C, DRX was observed to occur at a particular $\dot{\varepsilon}$, while the DRX temperature increased with decrease in the purity level of Al (Ravichandran and Prasad, 1991).

CONCLUSIONS

- The high temperature deformation behavior of Al-Cu-Mg alloy and Al-Cu-Mg alloy containing 0.06 wt.% of Sn was investigated by hot compression tests performed at temperatures ranging from 300 to 500°C and strain rates ranging from 0.001 to 1.0 sec^{-1}. Flow stress of both materials increased with increase in strain rate and decrease in deformation temperature
- From the point of design applicability, the Al-Cu-Mg alloy microalloyed with Sn, possesses higher strength, but is relatively difficult to deform as revealed from the higher values of flow stress
- Artificial neural network (ANN) modeling was carried out for the first time providing excellent prediction of flow stress at different combinations of strain, strain rate and temperature, during hot deformation of these wrought and microalloyed Al alloys
- From the flow stress data predicted by ANN modeling, power dissipation efficiency maps, instability maps and subsequently the processing maps were generated to delineate the process domains for safe metal working. This is the first attempt made to propose the optimum hot processing window providing an intelligent processing and manufacturing system for these wrought 2xxx series Al-Cu-Mg alloys microalloyed with Sn
- The power dissipation efficiency maps revealed a maximum efficiency of 60% for the base alloy without Sn content while a comparatively lower value of 40% for the alloy with trace addition of Sn. The instability maps generated for this alloy containing Sn revealed only one instability regime
- The safe regimes for hot working of the Al-Cu-Mg alloy without Sn content were observed at (i) very low strain rate (<0.003 sec^{-1}) with temperature <450°C and (ii) high temperature (>400°C) with strain rate >0.02 sec^{-1}. The safe processing zone of the microalloyed material is at low strain rate (<0.01 sec^{-1}) for the entire range of temperatures studied
- Considerable flow softening was observed after attaining the peak stress value in both the alloys deforming at low strain rate of 0.001 sec^{-1}. The phenomenon may be interpreted as a consequence of dynamic recovery (DRV) and dynamic recrystallization (DRX) which basically characterized the safe processing zones of both the alloys
- Metallurgical instability during hot deformation was observed to be driven by shear band formation and/or intercrystalline cracking for the investigated Al alloys

REFERENCES

ASM International Handbook Committee, 1990. Properties and Selection: Nonferrous Alloys and Special-Purpose Materials. ASM International, New York, USA., Pages: 1328.

Banerjee, S., P.S. Robi and A. Srinivasan, 2012. Prediction of hot deformation behavior of Al-5.9%, Cu-0.5%, Mg alloys with trace additions of Sn. J. Mater. Sci., 47: 929-948.

Banerjee, S., P.S. Robi, A. Srinivasan and P.K. Lakavath, 2010. Effect of trace additions of Sn on microstructure and mechanical properties of Al-Cu-Mg alloys. Mater. Des., 31: 4007-4015.

Cavaliere, P., 2002. Hot and warm forming of 2618 aluminium alloy. J. Light Metals, 2: 247-252.

Flynn, P.W., J. Mote and J.E. Dorn, 1961. On the thermally activated mechanism of prismatic slip in magnesium single crystals. Trans. Met. Soc., 221: 1148-1154.

Frost, H.J. and M.F. Ashby, 1982. Deformation Mechanism Maps. Pergamon Press, New York and Oxford.

Heinz, A., A. Haszler, C. Keidel, S. Moldenhauer, R. Benedictus, W.S. Miller, 2000. Recent development in aluminium alloys for aerospace applications. Mater. Sci. Eng. A, 280: 102-107.

Hirosawa, S., T. Sato, A. Kamio and H.M. Flower, 2000. Classification of the role of microalloying elements in phase decomposition of Al based alloys. Acta Mater., 48: 1797-1806.

Jonas, J.J., C.M. Sellars and T.W.J. McG, 1969. Strength and structure under hot-working conditions. Metall. Rev., 14: 1-24.

Kaibyshev, R., O. Sitdikov, I. Mazurina and D.R. Lesuer, 2002. Deformation behavior of a 2219 Al alloy. Mater. Sci. Eng. A, 334: 104-113.

Kutumarao, V.V. and T. Rajagopalachary, 1996. Recent developments in modeling the hot working behavior of metallic materials. Bull. Material Sci., 19: 677-698.

Liu, X.Y., Q.L. Pan, Y.B. He, W.B. Li, W.J. Liang and Z.M. Yin, 2009. Flow behavior and microstructural evolution of Al-Cu-Mg-Ag alloy during hot compression deformation. Mater. Sci. Eng. A, 500: 150-154.

Medina, S.F. and C.A. Hernandez, 1996. The influence of chemical composition on peak strain of deformed austenite in low alloy and microalloyed steels. Acta Mater., 44: 149-154.

Murty, S.V.S.N., B.N. Rao and B.P. Kashyap, 2000. Instability criteria for hot deformation of materials. Int. Mater. Rev., 45: 15-26.

Prasad, Y.V.R.K. and N. Ravichandran, 1991. Effect of stacking fault energy on the dynamic recrystallization during hot working of FCC metals: A study using processing maps. Bull. Mater. Sci., 14: 1241-1248.

Prasad, Y.V.R.K. and S. Sasidhara, 1997. Hot Working Guide: A Compendium of Processing Maps. ASM International, Materials Park, OH., ISBN: 9780871705983, Pages: 545.

Prasad, Y.V.R.K., 1990. Recent advances in the science of mechanical processing. Indian J. Technol., 28: 435-451.

Prasad, Y.V.R.K., H.L. Gegel, S.M. Doraivelu, J.C. Malas, J.T. Morgan, K.A. Lark and D.R. Barker, 1984. Modeling of dynamic material behavior in hot deformation: Forging of Ti-6242. Metallurgical Trans. A, 15: 1883-1892.

Prasad, Y.V.R.K., T. Seshacharyalu, S.C. Medeiors and W.G. Frazier, 2000. Effect of preform microstructure on the hot working mechanisms in ELI grade Ti-6Al-4V: Transformed βv. equiaxed (α+β). Material Sci. Technol., 16: 511-516.

Raj, R., 1981. Development of a processing map for use in warm-forming and hot-forming processes. Metallurgical Transact., 12A: 1089-1097.

Raju, P.N., K.S. Rao, G.M. Reddy, M. Kamaraj and K.P. Rao, 2007. Microstructure and high temperature stability of age hardenable AA2219 aluminium alloy modified by Sc, Mg and Zr additions. Mater. Sci. Eng. A, 464: 192-201.

Ravichandran, N. and Y.V.R.K. Prasad, 1991. Dynamic recrystallization during hot deformation of aluminium: A study using processing maps. Metallurgical Materials Transact. A., 22: 2339-2348.

Robi, P.S. and U.S. Dixit, 2003. Application of neural networks in generating processing map for hot working. J. Mater. Process Technol., 142: 289-294.

Sercombe, T.B. and G.B. Schaffer, 1999. On the use of trace additions of Sn to enhance sintered 2xxx series Al powder alloys. Mater. Sci. Eng. A, 268: 32-39.

Sukumaran, K., K.K. Ravikumar, S.G.K. Pillai, T.P.D. Rajan, M. Ravi, R.M. Pillai and B.C. Pai, 2008. Studies on squeeze casting of Al 2124 alloy and 2124-10% SiCp metal matrix composite. Mater. Sci. Eng. A, 490: 235-241.

Zhang, H., L. Li, D. Yuan and D. Peng, 2007. Hot deformation behavior of the new Al-Mg-Si-Cu aluminum alloy during compression at elevated temperatures. Mater. Charact., 58: 168-173.